Quenching Effects in Nitrogen Gas Scintillation

Hideki Morii, Kentaro Mizouchi, Tadashi Nomura, [1]
Noboru Sasao, Toshi Sumida

Department of Physics, Kyoto University, Kyoto 606-8502, Japan

Makoto Kobayashi

High Energy Accelerator Research Organization (KEK), Ibaraki 305-0801, Japan

Yoshiyuki Murayama [2] , Ryuichi Takashima

Department of Physics, Kyoto University of Education, Kyoto 612-8522, Japan

Abstract

We report on the studies of quenching effects in N_2 scintillation. Our main interest is to find out a practical gas which reduces scintillation yield in air substantially. We have studied O_2, CO_2, and CH_4 in N_2, and have determined their Stern-Volmer constant. When two quenching gasses are used at the same time, the effects are found to be additive. Quenching mechanism of these gasses is discussed and its practical application is reported.

PACS: 29.40.Mc

Key words: gas scintillation, quenching

1 Introduction

Nitrogen gas scintillation has been known to exist for a long time, and has been employed as a particle detector in many experiments [1] [2]. It is an essential phenomenon for these detectors, but is rather harmful for some applications. This is exactly the case for a detector we are now preparing. This detector, called a beam catcher, is a part of a bigger detector system in an experiment named KOPIO [3]. The experiment itself is to measure the branching ratio of $K_L \to \pi^0 \nu \bar{\nu}$ with a single event sensitivity of $\sim 6 \times 10^{-13}$. The beam catcher is placed inside a K_L beam, and its role is to distinguish high energy gamma rays (100-1000 MeV) coming with K_L and/or

[1] Corresponding author; e-mail: nomurat@scphys.kyoto-u.ac.jp
[2] Present address; FSIABC Inc, Kanagawa 247-0072, Japan

much abundant neutrons. The beam catcher itself will be detailed elsewhere. Below we briefly describe it to clarify our motivation of the study reported here. The beam catcher is composed of many identical modules; each module is essentially a sandwich calorimeter consisting of a lead plate, an aerogel tile, light collecting mirrors, and a photomultiplier tube (PMT). We note that there is an air gap between the aerogel and the mirror. The PMT detects the Cherenkov lights produced in the aerogel radiator by electrons and positrons of an electromagnetic shower. It is essential for the experiment to reduce as much as possible misidentification probability, i.e. the probability of detecting neutrons as gamma rays. This is the very reason we must employ a Cherenkov radiator with a low refractive index, instead of more common scintillator; it is relatively insensitive to heavy charged particles. As stated, there exists an air gap between the radiator and the light collecting mirror, and this would give background counts due to nitrogen scintillation. This scintillation yield can be completely neglected as long as the high-energy gamma ray detection is concerned. Namely, expected number of photoelectrons due to the N_2 scintillation is much smaller than that from Cherenkov photons created by the gamma rays of our interests. However, neutrons, which are by far the most abundant particles passing through the catcher module, would produce charged particles which in turn make scintillation lights in the air. The background signal observed in the PMT is expected to be single-photon random pulses; the PMT would behave as if it had an additional dark current source. Thus we simulated by the GEANT3 code to calculate this noise current, and concluded that at the worst case it results in unsatisfactory PMT operation such as high trigger rate and/or gain change etc. [1] It is thus desirable to reduce this background scintillation as much as practical; actually we set our goal to reduce it by a factor of 3$\sim$4, considering that it would then dominated by other intrinsic noise source produced by neutron reactions. We note that it is unpractical to install the aerogel and/or mirrors in a vacuum vessel. Thus the only way is to find a quenching gas to suppress the nitrogen scintillation.

The paper is organized as follows. Section 2 describes our experimental setup, data taking, and analysis procedures. In Section 3, the results are presented with discussions. Section 4 is devoted to the conclusions.

2 Experiment

2.1 Setup

The experimental setup is shown in Fig. 1. It consists of a gas-tight vessel made with two SUS404 pipes crossed each other, two 2 inch PMTs to view scintillation lights through the top and bottom quartz windows, an α-ray source attached at the head of a rod, a PIN photodiode (PD) to measure the kinetic energy of α particle, and a light emitting diode (LED) used to check and monitor the PMTs. The actual α-source is ^{241}Am; it emits 5.486 MeV (85%) and 5.443 MeV

[1] The ambiguity in the conclusion was due to uncertainties in the neutron spectrum and their interactions used in the simulation.

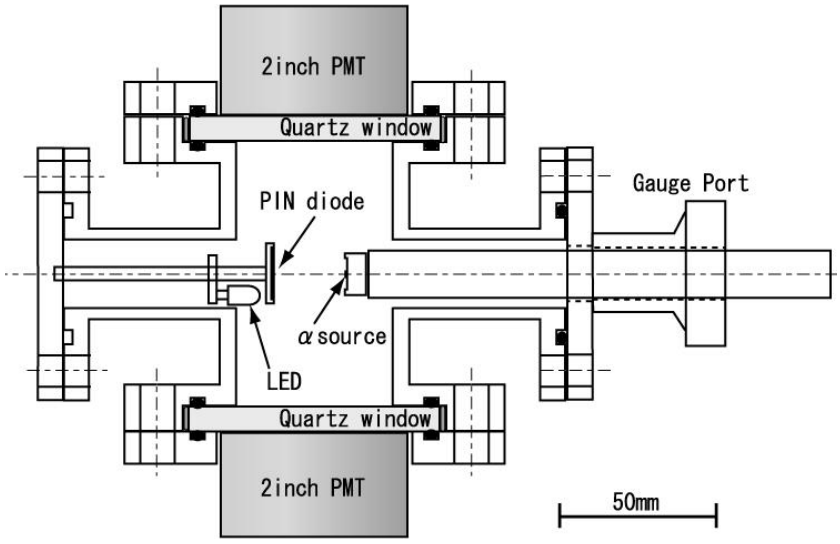

Fig. 1. Cross sectional view of experimental setup. α-particles emitted from ^{241}Am source lose their energy in gas and are caught by PIN diode (PD). Scintillation light is detected with two PMTs on the top and bottom of the vessel.

(13%) α-particles. The photodiode is Hamamatsu [4] S3590-09 [5], which has no protection layer on the injection surface. It is used to create a trigger signal upon detection of α-particles, and to measure their kinetic energy. The distance between the source and photodiode (denoted by L_{sp}) can be varied by pushing or pulling the rod. The PMTs in use are Hamamatsu R2256-02 and R329-02 [6]; they have a bialkaline cathode with quartz (R2256-02) or borosilicate glass (R329-01) window, respectively. Pure and mixed gasses are introduced to the vessel after evacuating it at least for 5 minutes. The mixing ratio is controlled by adjusting flow rate, and is monitored by gas flow meters. We estimate uncertainty on the gas mixing rate to be about 5%. All measurements are done at one atmospheric pressure.

2.2 Data acquisition system and data taking procedure

Fig. 2 shows a schematic diagram of our readout system. The PD signal is first amplified by a pre-amplifier, and then discriminated. The threshold level is set to 1.0 MeV. Its output is fed into two gate generators, which provide the gates to two types of analog-to-digital converters (ADC); one is a pulse-height sensitive ADC for the PD signal (1-μsec-long gate), and the other is a charge sensitive ADC for the PMTs (80-nsec-long gate). With a trigger signal, a data taking cycle is initiated by a computer, and all ADC data are read via a CAMAC system.

We prepare five kinds of gasses; nitrogen (N_2), dry air, oxygen (O_2), carbon dioxide (CO_2), and methane (CH_4). The mixing ratio is changed by a step of 10%. At one gas mixture, the source-photodiode distance (L_{sp}) is varied from 5 to 30 mm by a step of 5 mm. Each data point consists of about 40000 triggers.

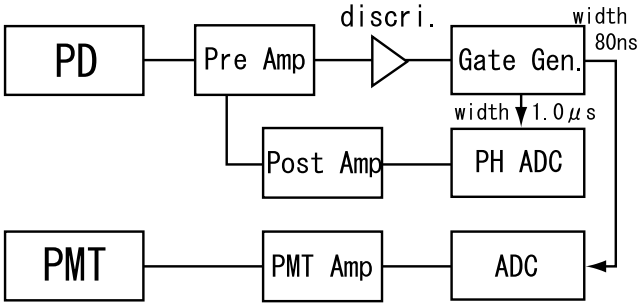

Fig. 2. Readout system in schematic diagram. Circuit is triggered by PD signal with a threshold level of 1.0 MeV in α-particle kinetic energy. With trigger, gate generators make two gates with different width (80nsec and 1μsec), and the ADC of PMT and PD are read.

In this subsection, we present our data analysis procedure, taking the data of pure nitrogen gas as an example. Fig. 3 shows an example of the PD pulse height distribution; this particular data is taken at $L_{sp} = 15$ mm. Fig. 4 shows corresponding ADC spectra for the PMTs. First of all,we fit a gaussian function to the PD spectrum, and require events to be inside $\pm 2\sigma$ region around the peak.

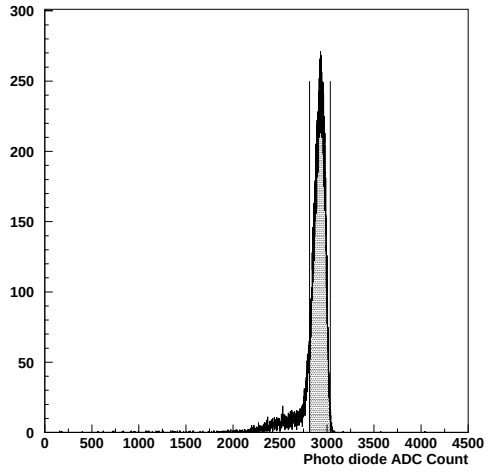

Fig. 3. Typical PD spectrum taken at $L_{sp} = 15$ mm, corresponding to 4.2 MeV in α-particle kinetic energy. Shaded area shows the $\pm 2\sigma$ region around the peak.

The two vertical lines in Fig. 3 indicate the cut boundaries. The lower (upper) curves in Fig. 4 are the PMT spectrum after (before) this cut. We then calculate the number of photoelectrons (n_{pe}) from this spectrum. To this end, we employ two different methods: one is to calculate inefficiency (the sharp peak on the left in Fig. 4), and the other is to calculate mean of the spectrum. In both cases, we assume the Poisson statistics to hold for the observed photoelectrons. In the former method, the inefficiency is expressed by

$$P_0 = \exp\left(- < n_{pe} >\right), \tag{1}$$

where P_0 represents the probability of observing no photoelectron (i.e. inefficiency), and $< n_{pe} >$ is the average number of photoelectrons. In reality, we define the inefficiency as the counts below the lowest point between the zero and single photoelectron peaks. For example, the shaded region in Fig. 4 shows the inefficiency counts.

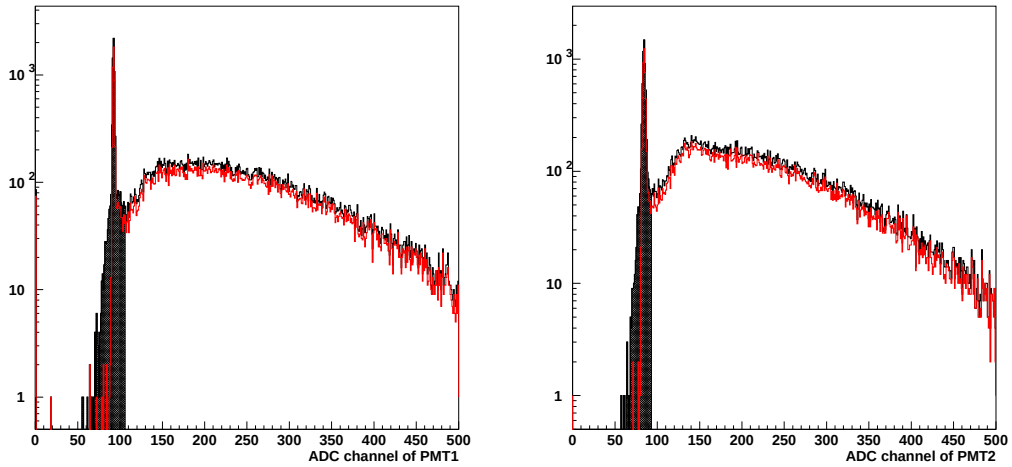

Fig. 4. Typical PMT spectrum taken at $L_{sp} = 15$ mm for PMT1 (left) and PMT2 (right). Shaded region shows the inefficiency counts.

In the latter method, we calculate the mean of the spectrum, and divide it by the one photoelectron peak channel, which is obtained by a separate calibration run with LED. The number of photoelectrons obtained in these methods are listed in Table1.

Table 1
Number of photoelectrons obtained in two methods for pure N_2 at $L_{sp} = 15$ mm.

Method	PMT1 (R2256-02)	PMT2 (R329-02)
inefficiency	2.01 ± 0.07	1.95 ± 0.08
single photoelectron	1.98 ± 0.04	1.95 ± 0.04

Two points are of our interest in the table. First of all, since PMT1 has wider spectrum sensitivity, it may observe in principle larger number of photoelectrons. In reality, the results from PMT1 and PMT2 agree well each other, indicating the N_2 scintillation is predominantly in the visible region where both PMT1 and PMT2 have identical sensitivity. We will discuss on this point in more detail in Section 3.1. The second point to be noted is agreement in the two measurement methods. The measurements at other distance and/or with other gas mixtures indicate they always yield consistent results. In the following, we quote only the results from the inefficiency method because the other method (single photoelectron) is found somewhat vulnerable to PMT gain change.

The next step in the analysis procedure is to deduce energy loss ΔE of α-particles in the gas. Fig. 5 shows the peak of the PD spectrum (such as shown in Fig. 3) as a function of L_{sp}. In this plot, the peak position at zero distance is assigned to 5.48 MeV. The solid curve is the result of GEANT3 simulations. As seen, they agree fairly well each other although a small discrepancy exists at large L_{sp}. We regard that the PD signal (measured value) represents the kinetic energy remained after the dE/dx loss in the gas. For example, at the distance of L_{sp}=15 mm, the α-particle loses the energy of $\Delta E = 5.48 - 4.20 = 1.28$ MeV in the gas.

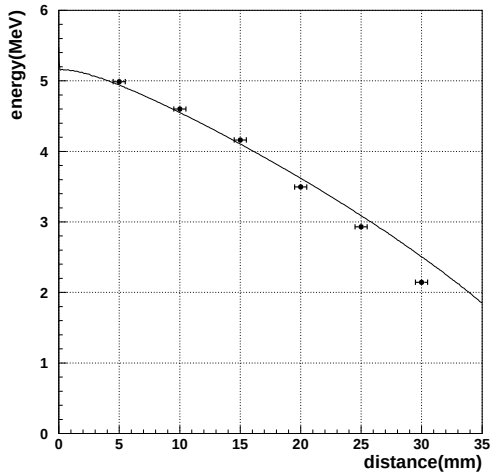

Fig. 5. PD peak as a function of L_{sp}. The horizontal error bars represent the uncertainty of α-source position. The vertical errors are negligibly small. The solid curve is the result of GEANT3 simulations.

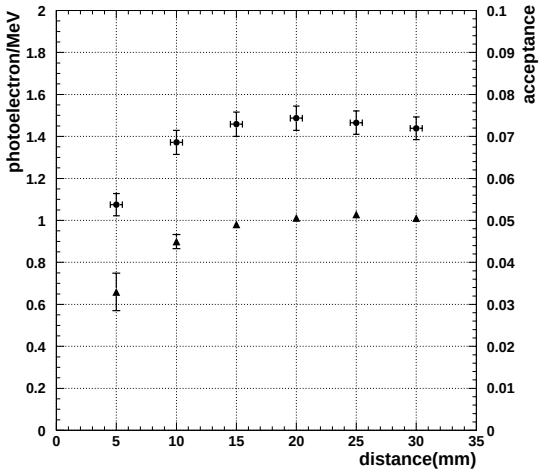

Fig. 6. Number of photoelectrons per 1MeV energy loss (solid dots with crossing error bars). The geometrical acceptance is shown by triangle points.

Fig. 6 shows the number of photoelectrons per unit energy loss, $n_{pe}/\Delta E$, as a function of L_{sp}. Also shown is a geometrical acceptance calculated with a simulation code. The vertical errors assigned to the data points represent the statistical errors, and the horizontal error shows a

uncertainty (± 0.5 mm) assigned to the location of the α-source (positioning error). The vertical errors assigned to the geometrical acceptance are the difference in acceptance when the source has the positioning error quoted above.

In order to calculate the total number of photons emitted by the gas per unit energy loss (dN_{ph}/dE), we need to know a quantum efficiency of the PMT photocathode and also the emission spectrum of the N_2 scintillation. For the sake of simplicity, we completely neglect the emission in the UV region (see table 1), and assume a flat spectrum in the visible region. Averaging over the quantum efficiency curve provided by Hamamatsu [7], we find the average value to be 20%. We estimate that this value, common to PMT1 and PMT2, has a scale error of at least 10% [2].

Fig. 7 shows the plot of dN_{ph}/dE versus L_{sp}. The errors come from statistics and those in the geometrical acceptance, which in turn stem from the α-source positioning uncertainty. They are combined in quadrature.

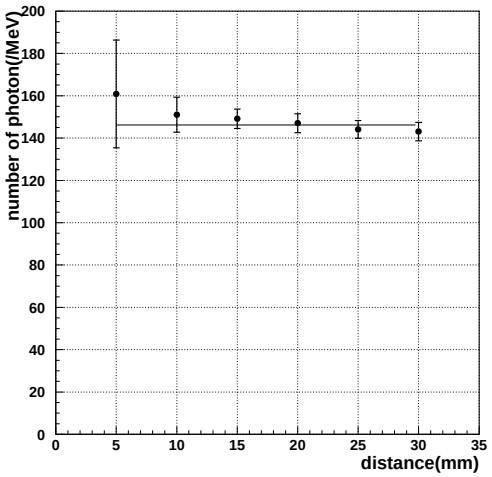

Fig. 7. dN_{ph}/dE as function of L_{sp}. The vertical errors represent statistical errors combined with the effect of α-source positioning uncertainty.

As expected, the measured points are independent of the distance L_{sp} [3]. We define the value $< dN_{ph}/dE >$ to be the best fit of these values; this is indicated by the horizontal line in Fig. 7. For the pure nitrogen, we find

$$\begin{aligned} < dN_{ph}/dE > &= 141.1 \pm 2.1 \quad (\mathrm{PMT1}) \\ &= 146.2 \pm 2.1 \quad (\mathrm{PMT2}). \end{aligned}$$

[2] This error estimate is partly supported by the compatibility of our assumption (no UV emission) with the data reported by the Duquesne and Kaplan [8]. For the large part, this is an educated guess by the past experiences.

[3] This particular data seem to have some systematic tendency by accident. However, the same data for other gas mixtures not have such tendency.

These values are consistent with the value given by Birks [9].

3 Results and Discussions

3.1 Scintillation Light Yield for pure gasses and air

In this subsection, we present our results for 4 pure gasses (N_2, O_2, CO_2, and CH_4) and dry air. In order to calculate photon yield, we need to know the emission spectrum for each gas at least in the visible region. Since we are unable to find it, below we simply use the same average quantum efficiency of 20% as that of N_2. Table 2 lists the values of $< dN_{ph}/dE >$ for 4 pure gasses and dry air.

Table 2
The number of scintillation photons per 1 MeV energy loss ($< dN_{ph}/dE >$)

Gas	PMT1 (R2256-02)	PMT2 (R329-02)
N_2	141.1 ± 2.1	146.2 ± 2.1
Air	25.46 ± 0.43	26.06 ± 0.461
O_2	0.61 ± 0.22	0.46 ± 0.22
CO_2	5.09 ± 0.28	4.90 ± 0.27
CH_4	1.39 ± 0.09	1.32 ± 0.08

As can be seen from the table 2, there is no big difference between PMT1 and PMT2 for all gasses, justifying the assumption that the emission is predominantly in visible region. Hereafter, we only quote the results from PMT2, considering that we will actually use this type of photocathode and window material.

3.2 Quenching Effect in pure Nitrogen

In this subsection we show the results of quenching effect in pure N_2. When quencher gas (oxygen, for example) is mixed into pure nitrogen, energy transfer such as N_2^* + $O_2 \rightarrow N_2$ + O_2^* occurs and O_2^* decays non-radiatively. This mechanism, called quenching, reduces the light yield of scintillation. If the fraction of the quencher gas is small, quenching effect is represented by a model due to Stern and Bolmer [10], expressed by

$$N_{ph} = \frac{N_{ph}^0(N_2)}{1 + Kc}, \tag{2}$$

where $N^0_{ph}(N_2)$ represents the light yield from pure nitrogen, K the Stern-Volmer constant and c the fraction of the quenching gas. The constant K measures the power of quenching effect.

A phenomenological model can be developed to extend the original Stern-Volmer equation applicable to the full range of c. The derivation of the model can be found in Appendix, together with a brief description of the original model. The modified model is expressed as

$$N_{ph} = \frac{1}{1+Kc}(1-c)N^0_{ph}(N_2) + [1 + A(1-c)]cN^0_{ph}(Q), \tag{3}$$

where $N^0_{ph}(Q)$ is the light yield by pure quencher gas and A measures the effect of energy transfer from quencher gas to radiative excited status of N_2. Fig. 8 shows the measurement results obtained for the N_2-O_2 gas mixture.

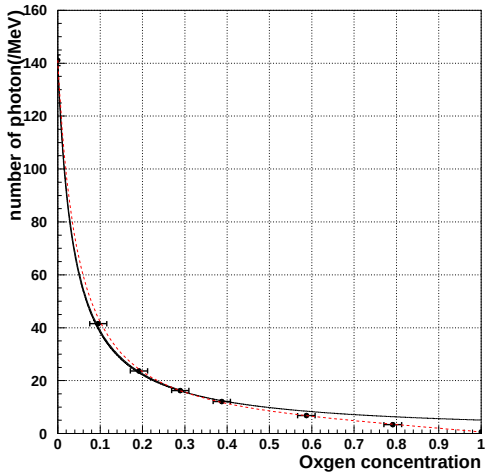

Fig. 8. O_2 quenching effect in N_2. The solid and dashed curves show the fit with the original Stern-Volmer and modifies Stern-Volmer models, respectively.

The ordinate represents $< dN_{ph}/dE >$ while the abscissa is the fraction of oxygen gas. The solid curve shows a fit to the data points with eq. (2) up to the oxygen concentration of 40% ($c = 0 \sim 40\%$) and the dashed curve shows a fit with eq. (3). In both fits, we assume $N^0_{ph}(N_2)$ or $N^0_{ph}(Q)$ is given by the data point at $c = 0$ or $c = 1$, respectively. Thus, the free parameters are only K and/or A in the fit. We find K of eq. (2) to be $K = 26.2 \pm 1.5$ for O_2 in N_2, which is consistent with the value of Birks [9]. In modified model, we find K to be $K = 20.7 \pm 1.5$ and parameter A to be $A = 8.2 \pm 2.1$. Fig. 9 (Fig. 10) shows the same plot for the mixture of N_2 and CO_2 (N_2 and CH_4), together with the curves obtained by a similar procedure. In all cases, the modified Stern-Volmer model (eq. (3)) reproduces the data points very well in the full range of c. We summarize the results in table 2, in which χ^2/ν represents the chi-square per degree of freedom in the fit [4].

[4] The values of χ^2 are all small compared with their expected value of ν. This fact indicates possible overestimate of errors assigned to the data points. However, we leave as they are because the fits seem satisfactory judging from Fig. 8 - Fig. 10.

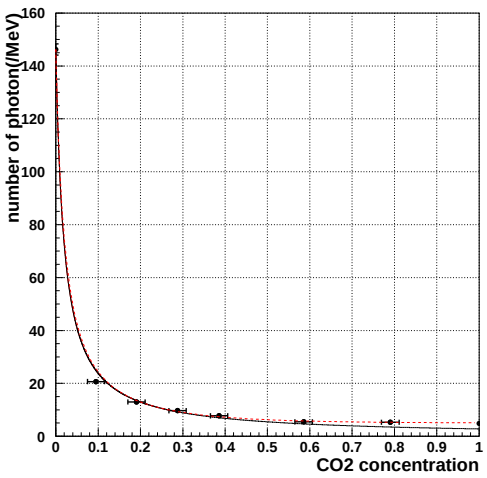

Fig. 9. CO_2 quenching effect in N_2. The solid and dashed curves show the fit with the original Stern-Volmer and modifies Stern-Volmer models, respectively.

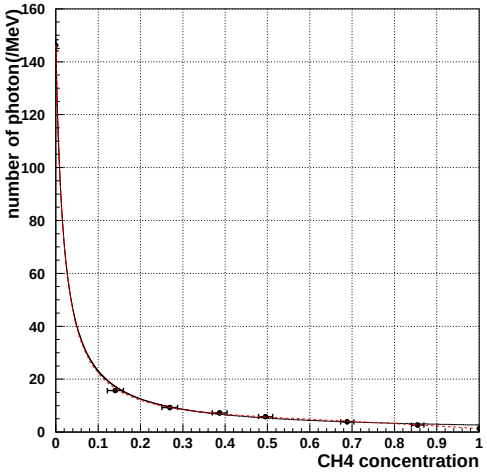

Fig. 10. CH_4 quenching effect in N_2. The solid curve and dashed curve show the fit with Stern-Volmer and modified Stern-Volmer, respectively.

3.3 Quenching Effect in Air

In this subsection, we present the results of quenching effect in the case that quencher gas is mixed in air. Because we just measure low c region in this case, we use the original Stern-Volmer model expressed by eq. (2). For the mixture of three gasses, the quenching effect is expected to work additively. Thus, eq. (2) can be modified to

$$N_{ph} = \frac{N_{ph}^0}{1 + K_1 c_1 + K_2 c_2}, \tag{4}$$

Table 3
The Stern-Volmer constant K in pure nitrogen. In the original model, the fit range is $c = 0 \sim 40$ %, and in the modified model, $c = 0 \sim 100$ %.

	original Stern-Volmer (eq. (2))		modified Stern-Volmer (eq. (3))		
Quencher Gas	K	χ^2/ν	K	A	χ^2/ν
O_2	26.4 ± 1.5	1.0 / 3	20.7 ± 1.5	7.1 ± 2.1	1.4 / 4
CO_2	48.5 ± 3.0	1.6 / 3	45.7 ± 4.0	2.6 ± 1.7	3.7 / 4
CH_4	53.3 ± 2.7	1.8 / 3	51.8 ± 5.1	9.3 ± 1.8	1.0 / 4

where the suffixes 1 and 2 distinguish the gas species. In the case that a quenching gas is added to the air, quenching effect is sum of the oxygen and quencher gas. We investigate the quenching effects in air, hoping to find out appropriate gas mixture usable in the actual experiment. Fig. 11 and Fig. 12 shows the measurement results obtained for the Air-CO_2 and Air-CH_4 gas mixture, respectively. The ordinate and abscissa are the same as in Fig. 8, and the solid curve shows

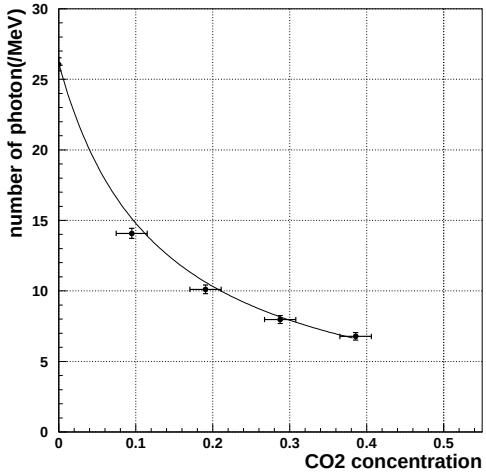

Fig. 11. CO_2 quenching effect in Air. Solid curve shows the fit with eq. (4).

a fit to the data points with a function eq. (4). In the fit, the value for K_1c_1 is fixed at the value obtained by the N_2-O_2 measurement: $K_1c_1 = (26.2 \pm 1.5) \times 0.2 = 5.2 \pm 0.3$. We find $K_{CO2} = 45 \pm 4$ for CO_2, and $K_{CH4} = 53 \pm 2$ for CH_4. These results are consistent with the value measured with nitrogen. The Stern-Volmer constants measured in air are summarized in Table 3. From Fig. 11 and Fig. 12, we conclude that we need to mix 30% of CO_2 or 20% of CH_4 to reduce the scintillation due to the air by a factor of 3. The agreement between the corresponding values for K in table 3 and table 4 indicates the validity of the assumption that quenching effect is additive in these gasses.

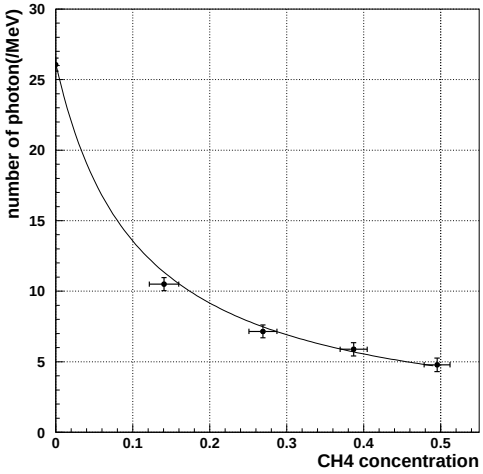

Fig. 12. CH_4 quenching effect in Air. Solid curve shows the fit with eq. (4).

Table 4
The Stern-Volmer constant K (fit with eq. (4)) in dry air.

Quencher Gas	K	χ^2/ν
CO_2	43 ± 3	3.2 / 4
CH_4	52 ± 4	2.6 / 4

4 Conclusions

In this paper, we have presented the measurement of quenching effect in N_2 gas scintillation. The quenching gas studied are O_2, CO_2 and CH_4. Among these gasses, the CH_4 gas is the most effective. We find the quenching effect can be well represented by a phenomenological model of eq. (3) for a full range of quencher gas concentration c. When the two quenching gas are used in N_2, the effect seems to be additive. The quenching effect occurs most likely due to energy exchange by collisions between the gas molecules. As to our original motivation of the study, we are now confident that the N_2 scintillation background can be reduced to a tolerable level by adding CO_2 or CH_4 gas in the air.

Acknowledgements

This research was supported by the Ministry of Education, Culture, Sports, Science and Technology of Japan, under the Grant-in-Aids for Scientific Research on Priority Areas, and through the Japan-U.S. Cooperative Research Program in High Energy Physics.

References

[1] W. Tornow, H. Huck, H. J. Kober and G. Nertens, *Nucl. Instr. and Meth.*, **133**, 435 (1976)

[2] M. Mutterer, J. P. Theobald, and K. P. Schelhaas, *Nucl. Instr. and Meth.*, **144**, 159 (1977)

[3] http://pubweb.bnl.gov/people/e926/

[4] Hamamatsu Photonics K.K., Iwata-country, Shizuoka Pref., 438-0193 Japan

[5] Hamamatsu Catalog, *Si PIN photodiode S3590 series* (Catalog No. KPIN10521)

[6] Hamamatsu Catalog, *Photomultiplier Tube R329-02* (Catalog No. TPMH1254E01)

[7] Hamamatsu Catalog, *Photomultiplier Tubes and Assemblies For Scintillation Counting & High Energy Physics* (Catalog No. TPMO0001E06)

[8] Duquesne, M. and Kaplan, I., *J. Phys. Radium*, **21**, 708 (1960)

[9] J. B. Birks, *The Theory and Practice of Scintillation Counting*, Pergamon Press, Oxford (1964) p.570-614

[10] Stern,O. and Volmer,M., *Phys. Z.*, **20**, 183 (1919)

A Stern-Volmer model

A.1 Stern-Volmer model

In this appendix, we derive the Stern-Volmer model by treating quenching mechanism phenomenologically. Here, we deal with the simplest situation: one quencher gas is mixed in N_2. Let us assume only one excited state of N_2 is involved in scintillation, and decays through one of four deexcitation modes: radiation (k_f), internal quenching (k_i), collisional quenching with N_2 (k_{qN_2}) or collisional quenching with quencher (k_{qQ}). The rate parameter (1/sec) for each process is denoted by the quantity in the parentheses. Then, the total rate (k) can be expressed as

$$k = k_f + k_i + k_{qN_2}(1-c) + k_{qQ}c, \tag{A.1}$$

where c is the concentration of quencher gas.
The scintillation efficiency ϵ can be represented by

$$\epsilon = \frac{k_f}{k} = \frac{k_f}{k_f + k_i + k_{qN_2}(1-c) + k_{qQ}c}. \tag{A.2}$$

The number of the emitted photon due to N_2 excitation is proportional to ϵ and the number of N_2^*. A straightforward calculation leads to

$$N_{ph}(N_2) = (1-c)\frac{1}{1+Kc}N_{ph}^0(N_2). \tag{A.3}$$

where $K = (k_{qQ} - k_{qN_2})/(k_f + k_i + k_{qN_2})$ is introduced for simplicity, and $N_{ph}^0(N_2)$ is the number of emitted photons when $c = 0$ (pure N_2).

Usually the Stern-Volmer equation is quoted as

$$N_{ph}(N_2) = \frac{N_{ph}^0(N_2)}{1+Kc}. \tag{A.4}$$

which is valid when $c \ll 1$.

A.2 modified Stern-Volmer model

In order to make the Stern-Volmer model applicable to all range of quencher concentration c, we introduce light emission mechanism induced by quencher gas. Here, we assume the excited quencher gas Q^* deexcites through five modes: fluorescence (k'_{fQ}), internal quenching (k'_i), collision with N_2 decaying radiatively (k'_{fN_2}), or non-radiatively (k'_{qN_2}), and collisional quench with quencher gas itself (k'_{qQ}). The rate equation can be written as

$$k' = k'_{fQ} + k'_i + k'_{fN_2}(1-c) + k'_{qN_2}(1-c) + k'_{qQ}c, \tag{A.5}$$

where k' is total rate for the excited quencher gas.
The scintillation efficiency ϵ' for Q^* becomes

$$\epsilon' = \frac{k'_{fQ} + k'_{fN_2}(1-c)}{k'} \tag{A.6}$$

Again, a straightforward calculation leads to

$$N_{ph}(Q) = \frac{c + K'c(1-c)}{1+K''(1-c)}N_{ph}^0(Q). \tag{A.7}$$

where $N_{ph}(Q)$ is the number of emitted photons by the excited states of quencher Q^*, and $N_{ph}^0(Q)$ is that corresponding to $c = 1$. The parameter K' and K'' are some simple functions of the rate parameters.

The total number of emitted photons N_{ph} is the sum of $N_{ph}(N_2)$ and $N_{ph}(Q)$; from eq. (A.3) and eq. (A.7), we can write N_{ph} as

$$N_{ph} = (1-c)\frac{1}{1+Kc}N^0_{ph}(N_2) + \frac{c+K'c(1-c)}{1+K''(1-c)}N^0_{ph}(Q). \tag{A.8}$$

In our actual fitting procedure, we further simplify the above equation to

$$N_{ph} = \frac{1}{1+Kc}(1-c)N^0_{ph}(N_2) + [1+A(1-c)]cN^0_{ph}(Q). \tag{A.9}$$

which is valid when $c \sim 1$.

Finally we note two comments. First, N_2^* may decay in principle into a radiative mode of the quencher gas. But in reality the process can be neglected compared with the main N_2 fluorescence mode. Second, in the eq. (A.9), the second term is inaccurate in the region of $c < 1$; however, the first term dominates in this region in any case. Thus we expect the equation to hold for all range of c to a good approximation.